

# Flame Stretch Interactions of Laminar Premixed Hydrogen/Air Flames at Normal Temperature and Pressure

K. T. AUNG, M. I. HASSAN, AND G. M. FAETH\*

Department of Aerospace Engineering, The University of Michigan, Ann Arbor, Michigan 48109-2118

Effects of positive flame stretch on the laminar burning velocities of hydrogen/air flames were studied both experimentally and computationally, considering freely (outwardly) propagating spherical laminar premixed flames. Measurements were based on motion picture shadowgraphy, while numerical simulations were based on typical contemporary chemical reaction mechanisms. Flame conditions studied included hydrogen/air flames having fuel-equivalence ratios in the range 0.3–5.0 at normal temperature and pressure. Both measured and predicted ratios of unstretched (plane flames) to stretched laminar burning velocities varied linearly with Karlovitz numbers over the test range (Karlovitz numbers up to 0.4), yielding Markstein numbers that were independent of Karlovitz numbers for a particular reactant mixture. Markstein numbers were in the range –1 to 6, with unstable (stable) preferential-diffusion conditions observed at fuel-equivalence ratios below (above) roughly 0.7. Present stretch-corrected laminar burning velocities were in reasonably good agreement with other determinations of laminar burning velocities at fuel-lean conditions where Markstein numbers, and thus effects of stretch, are small. In contrast, the stretch-corrected laminar burning velocities generally were smaller than other measurements in the literature at fuel-rich conditions, where Markstein numbers, and thus effects of stretch, are large. Finally, predicted unstretched laminar burning velocities and Markstein numbers were in reasonably good agreement with measurements, although additional study to improve the comparison between predictions and measurements at fuel-rich conditions should be considered. © 1997 by The Combustion Institute

## NOMENCLATURE

$D$	mass diffusivity
$K$	flame stretch
$Ka$	Karlovitz number, $KD_u/S_L^2$
$L$	Markstein length, Eq. 1
$Ma$	Markstein number, $L/\delta_D$
$P$	pressure
$r_f$	flame radius
$S_L$	laminar burning velocity based on unburned gas properties
$S_{L\infty}$	values of $S_L$ at largest radius observed
$t$	time
$T$	temperature
$\delta_D$	characteristic flame thickness, $D_u/S_L$
$\rho$	density
$\phi$	fuel-equivalence ratio

## Subscripts

$b$	burned gas properties
max	maximum observed value

$u$	unburned gas properties
$\infty$	asymptotic condition for an unstretched (plane flame)

## INTRODUCTION

Recent experimental studies of the effects of flame stretch on laminar premixed hydrogen/oxygen/nitrogen and hydrocarbon/air flames in this laboratory [1–3] were extended to consider hydrogen/air flames at normal temperature and pressure (NTP). Experimental observations of freely (outwardly) propagating spherical laminar premixed flames were used to find laminar burning velocities as a function of flame stretch (represented by the Karlovitz number), the sensitivity of laminar burning velocities to flame stretch (represented by the Markstein number), and the fundamental laminar burning velocities of unstretched (plane) flames. In addition, the measurements were used to evaluate recently proposed detailed  $H_2/O_2$  chemical reaction rate mechanisms due to Yetter and co-workers [4, 5], Wang and Rogg [6], and Frenklach et al. [7], based on corresponding detailed numerical simulations of freely (outwardly) propagating spherical

\* Corresponding author: G. M. Faeth, Department of Aerospace Engineering, The University of Michigan, 3000 FXB, 1320 Beal Avenue, Ann Arbor, MI 48109-2118 (E-mail: gmfaeth@umich.edu).

laminar premixed flames for the present test conditions.

The fact that interactions between the preferential diffusion of heat and various species (mass) and flame stretch influence the structure, stability, and speed of laminar premixed flames has been recognized for some time; see Clavin [8], Peters [9], and Law [10] for detailed reviews discussing these effects. A surprising finding of recent studies [1–3, 11–21], however, is that preferential-diffusion/stretch interactions are unusually strong, causing as much as an order of magnitude variation of laminar burning velocities in some instances, even for modest levels of stretch well away from conditions where significant effects of quenching might be anticipated. These observations suggest that the existing fundamental data base of laminar burning velocities, which is important for understanding flame properties and for evaluating and calibrating detailed chemical reaction mechanisms for flame environments, should be assessed for effects of stretch that are invariably present for practical flames in normal-gravity environments. In addition, the sensitivity of premixed laminar flames to stretch (represented by the Markstein number) provides a new and potentially sensitive flame parameter that should be studied and exploited in order to better understand premixed flames and to help evaluate detailed chemical reaction mechanisms for flames. Finally, information about laminar-burning-velocity/stretch interactions is needed to interpret and model interactions between flame surfaces and turbulence within the wrinkled thin laminar flamelet regime of premixed turbulent flames; see Ref. 1 and references cited therein.

A number of methods have been proposed to represent preferential-diffusion/stretch interactions of laminar premixed flames and to reduce measurements of flame properties to find these interactions; see Refs. 1–3, 8, 9, 16–22, and references cited therein for examples. Pending a generally agreed-upon resolution of this problem, however, present observations were analyzed to find preferential-diffusion/stretch interactions in the same way as earlier work in this laboratory for freely (outwardly) propagating spherical laminar premixed flames [1–3]. Several advantages moti-

vated this approach, aside from consistency with past work in this laboratory, as follows:

The results are found from fundamental measurements of flame position as a function of time and standard computations of the adiabatic flame properties of unstretched spherical laminar premixed flames, and they do not depend on predictions of flame structure using current models that are likely to change as the treatment of the transport and chemical kinetic properties of these flames improve in the future.

The results are concise so that all the experimental findings can be summarized by a few parameters in a table, facilitating their use by others in the future as concepts of preferential-diffusion/stretch interactions evolve.

The results can be inverted readily to find the propagation properties of stretched flames, which is helpful for interpreting the properties of turbulent premixed flames in the thin laminar flamelet regime and for selecting experimental conditions for turbulent premixed flames in this regime that minimize potential complications due to preferential-diffusion/stretch interactions.

The results provide a simple characterization of stable and unstable flame surface conditions with respect to effects of preferential diffusion.

It should also be noted that use of this approach does not affect present objectives to examine current capabilities to numerically simulate laminar premixed flames in order to predict effects of preferential-diffusion/stretch interactions, because both measurements and predictions are treated in the same way.

There is wide recognition that effects of flame thickness variations, curvature, and unsteadiness complicate the definition of laminar flame speed as well as measurements of effects of flame stretch on laminar burning velocities, even for seemingly simple freely (outwardly) propagating spherical laminar premixed flames [8, 23–26]. In order to minimize these difficulties, a relatively conservative approach was adopted when present flame conditions were selected for processing to find preferential-

diffusion/stretch interactions. In particular, processing was limited to conditions where  $\delta_D/r_f \ll 1$  in order to control effects of varying flame thickness, curvature, and unsteadiness, as discussed in Ref. 2, even though this precluded consideration of interesting flame properties near flammability limits and quenching (or extinction) conditions. Similarly, present observations were limited to conditions where effects of ignition disturbances and radiative heat losses were small, in order to control experimental uncertainties as discussed later.

Within the limitations just mentioned, the relationship between laminar burning velocity and flame stretch was based on an early proposal of Markstein [22], after later generalization and extension at the limit of small stretch as discussed by Clavin [8], as follows [2]:

$$S_L = S_{L\infty} - LK, \quad (1)$$

where  $S_L$  is the rate of propagation of the flame relative to the unburned gas,  $S_{L\infty}$  is the value of  $S_L$  for a plane flame where the flame stretch  $K = 0$ , and the coefficient  $L$  is a measure of the response of the flame to stretch, called the Markstein length [8]. Although the development of Eq. 1 is based on the considerations at the limit of small stretch, following Refs. 1–3 no such limitation is implied here due to the large variations of  $S_L$  that were observed during present measurements. As a result, a linear relationship between  $S_L$  and  $K$  (implying  $L$  independent of  $K$ ) should not be inferred from Eq. 1. In fact, past observations generally find a nonlinear relationship between  $S_L$  and  $K$  for available ranges of  $K$  and a variety of reaction mixtures; see Refs. 1–3 and 21, among others.

Proceeding from Eq. 1, the “local conditions” hypothesis is adopted [1, 2] where the flame response to effects of preferential diffusion is represented by local characteristic length and time scales for the diffusion phenomena of the stretched flame,  $\delta_D$  and  $\delta_D/S_L$ , rather than by corresponding scales at asymptotic conditions having small stretch where the magnitude of these scales can be very different. Dimensionless Karlovitz and Markstein numbers are defined to characterize flame

stretch and the response of a flame to stretch, as follows, based on these scales [1–3]:

$$Ka = K\delta_D/S_L, \quad Ma = L/\delta_D. \quad (2)$$

Then, substituting Eq. 2 into Eq. 1 and rearranging yields the dimensionless relationship between the laminar burning velocity and flame stretch [1]

$$S_{L\infty}/S_L = 1 + Ma Ka. \quad (3)$$

Similar to the discussion of Eq. 1, no fundamental linearity between  $S_{L\infty}/S_L$  and  $Ma$  (implying  $Ma$  independent of  $Ma$ ) should be inferred from Eq. 3. Nevertheless, constant values of  $Ma$  generally have been observed for values of  $Ma$  not too near extinction conditions and a variety of fuel mixtures, which helps to provide concise characterization of preferential-diffusion/stretch interactions [1–3].

In order to complete the present representation of preferential-diffusion/stretch interactions, the characteristic flame thickness  $\delta_D$  must be specified in the definition of  $Ma$  and  $Ma$  in Eq. 2. Many options are available to define  $\delta_D$  because it could be based on relative velocities at various points in the flames, on the mass diffusivities of any one of numerous species pairs present in the flames, or on the thermal diffusivity of the mixture within the flames, with the mass and thermal diffusivities additionally varying significantly with position within the flames. Fortunately, although the choice of  $\delta_D$  affects the magnitudes of  $Ma$  and  $Ma$  found from Eq. 2, it is not crucial to the representation of preferential-diffusion/stretch interactions because only the product,  $Ma Ka$ , affects  $S_{L\infty}/S_L$  and  $\delta_D$  actually cancels out of this product. Thus, both for convenience and for consistency with past work in this laboratory,  $\delta_D$  was based on the laminar burning velocity and the mass diffusivity of the fuel in the unburned gas [1, 2], as

$$\delta_D = D_u/S_L. \quad (4)$$

For the present conditions, involving hydrogen combustion in air, the binary diffusivities of the fuel with respect to nitrogen and oxygen are nearly the same while nitrogen is the main constituent of the nonfuel gases in the reactant mixture. Therefore, the binary diffusivity of the

fuel with respect to nitrogen was used to find  $D_u$ , similar to past work [1–3].

It is of interest to examine the present formulation at the limit of small stretch by expanding Eq. 3 at this limit to obtain

$$S_L/S_{L\infty} = 1 - Ma_\infty Ka_\infty \quad (5)$$

to leading order, where  $Ma_\infty$  and  $Ka_\infty$  are found from Eq. 2 after replacing  $S_L$  by  $S_{L\infty}$ . This form corresponds to the classical result from asymptotic theories [8], aside from the different convention for  $D_u$  which is trivial to remove, as discussed earlier. Thus, Eq. 3, which is used here in an attempt to find a concise treatment of preferential-diffusion/stretch interactions for conditions where effects of stretch are large [2], is consistent with asymptotic analysis of stretched premixed laminar flames at the limit of small stretch [8].

As mentioned earlier, the present approach to characterize effects of flame stretch on laminar burning velocities is not unique (see Refs. 8, 9, 16–22, and references cited therein for examples of alternatives), but it has several advantages for present use, pending development of generally accepted methods to treat these interactions when values of  $S_{L\infty}/S_L$  vary significantly from unity:

The present results are found directly without the involvement of flame structure models that are difficult to completely define and are likely to change as the technology base for flame structure predictions improves.

The present characterization of effects of stretch is concise which facilitates the use of the results by others in the future.

The positive and negative ranges of the present Markstein numbers provide a direct characterization of stable and unstable flame surface conditions with respect to preferential-diffusion effects.

It will be seen that the present results can be readily transformed to provide direct comparisons with earlier results by others concerning effects of flame stretch on hydrogen/air laminar premixed flame properties at NTP, e.g., Refs. 17, 18, 20, and 21.

Nevertheless, present considerations only address freely (outwardly) propagating spheri-

cal laminar premixed flames when  $\delta_D/r_f \ll 1$  and effects of ignition disturbances and radiation are small. The limitations of this approach for treating the general preferential-diffusion/stretch interactions of the laminar premixed flames are not known and clearly merit additional study.

Several previous investigations have considered the preferential-diffusion/stretch interactions of laminar premixed hydrogen air flames, e.g., Law and co-workers [11–13], Dowdy et al. [16], Taylor [17], and Mishra et al. [20]. Law and co-workers [11–13] measured the laminar burning velocities of hydrogen/air mixtures at normal temperature and pressures of 0.2–2.25 atm using the opposed-jet laminar premixed flame test configuration. These measurements involved an empirical extrapolation procedure to estimate the fundamental laminar burning velocity of an unstretched (plane) flame from measurements at finite levels of stretch, and they represent the first attempt to apply stretch corrections to laminar burning velocities. The resulting measurements were used to evaluate numerical simulations of unstretched laminar burning velocities based on a modified version of the Yetter et al. [4] reaction mechanism, among others, finding that improvements of the reaction mechanisms were needed. Nevertheless, it is of interest to extend the pioneering work of Law and co-workers [11–13] because these measurements were limited to fuel-lean conditions, the extrapolation scheme used requires evaluation using alternative methods, and the results provided neither experimental nor computational information about flame sensitivity to stretch, i.e., the Markstein numbers.

The study of Taylor and co-workers [16, 17] had similar objectives and scope as the present investigation. In particular, freely (outwardly) propagating spherical laminar premixed flames of hydrogen/air mixtures at NTP were observed in order to find both unstretched laminar burning velocities and the sensitivity of the flames to stretch represented by Markstein lengths at the limit of small stretch. A phenomenological analysis was used to assist data reduction, yielding a different procedure from the approach used here, to find unstretched laminar burning velocities and Markstein

lengths and to gain insight about the effects of low stretch rates on laminar flame propagation. This approach was motivated by earlier asymptotic analyses [8, 25] and sought to minimize uncertainties about effects of finite flame thickness, curvature, and unsteadiness when reducing measurements to find unstretched laminar burning velocities and Markstein lengths. Taylor and co-workers [16, 17] also undertook detailed numerical simulations of their outwardly propagating spherical flames, developing an  $H_2/O_2$  chemical reaction rate mechanism that provided very good estimates of their measurements of both unstretched laminar burning velocities and Markstein lengths. Due to the importance of the  $H_2/O_2$  reactant system, however, independent verification of these experimental and computational results is needed, along with additional consideration of the effect of stretch on Markstein lengths (or Markstein numbers).

The third earlier investigation involved the computational study of  $H_2/O_2/N_2$  flames by Mishra et al. [20, 21]. These investigators undertook numerical simulations of outwardly propagating spherical flames by considering conditions corresponding to the measurements of Kwon et al. [1] and Taylor and co-workers [16, 17]. These calculations were based on the  $H_2/O_2$  chemical reaction mechanism of Warhaft [27]. Predictions were reduced to illustrate  $S_L/S_{L\infty}$  as a function of Karlovitz numbers, which were normalized by characteristic length and time scales for an unstretched (plane) flame (and based on the thermal diffusivity of the unreacted mixture), as illustrated by Eq. 5. Given  $S_L/S_{L\infty}$ , a Karlovitz number, and the diffusivity used to define  $\delta_D$ , it is a trivial matter to transform results between the present study and those of Refs. 20 and 21. However, as noted earlier, the present approach provides a more concise treatment of flame response to stretch. An encouraging degree of agreement between the predictions and the measurements was observed by Mishra et al. [20, 21] in some instances; however, the evaluation was limited to just a portion of the available measurements so that a more complete assessment of the predictions is needed.

In view of the current status concerning the preferential-diffusion/stretch interactions of

premixed hydrogen/air flames, the objectives of the present study were as follows: (1) to complete new measurements of outwardly propagating spherical flames of hydrogen/air mixtures at NTP, (2) to complete corresponding numerical simulations of the test flames, (3) to reduce both the measurements and the numerical simulations to find characteristic laminar flame properties ( $S_{L\infty}$ , Ma, and the maximum value of Karlovitz number for the data,  $Ka_{max}$ ), (4) to compare the measurements and predictions with each other and with earlier results in the literature, and (5) to exploit the predictions of flame structure to gain insight about effects of flame/stretch interactions. Present measurements were limited to conditions where  $\delta_D/r_f \ll 1$  in order to avoid problems of flame unsteadiness and curvature [2], which implies that phenomena near flammability limits and quenching conditions could not be assessed. Nevertheless, significant effects of preferential-diffusion/stretch interactions were still observed over the available range of test conditions. Chemical reaction mechanisms considered during the numerical simulations included those of Yetter and co-workers [4, 5], Wang and Rogg [6], and Frenklach et al. [7], which represent typical methods used relatively widely in the literature.

The present discussion begins with descriptions of experimental and computational methods. Results are then considered, treating flame evolution and stability, burning velocity/stretch interactions, Markstein numbers, unstretched laminar burning velocities, sensitivity analysis of the chemical reaction mechanisms, and flame structure/stretch interactions, in turn.

## EXPERIMENTAL METHODS

### Apparatus

The present experiments were carried out in a spherical chamber having a volume of  $0.024\text{ m}^3$  and an inside diameter of 360 mm. Optical access was provided by two 100 mm diameter quartz windows mounted opposite one another. The chamber was capable of operation over a pressure range extending from complete vacuum up to a maximum of 34 atm.

The reactant mixture was prepared within

the chamber by adding gases at appropriate partial pressures to reach an initial pressure of 1 atm. All motion of the test gases during mixing was allowed to decay so that the gas was motionless when ignited. After combustion was complete, the chamber was vented to the laboratory exhaust system and then purged with dry air to remove condensed water vapor prior to refilling for the next test.

The combustible mixture was spark ignited at the center of the chamber using electrodes extending from the top and the bottom. One electrode was fixed while the other could be moved with a micrometer having a positioning accuracy of 10  $\mu\text{m}$ . The tips of the electrodes were fine wires (tungsten wire having a diameter of 250  $\mu\text{m}$  and a free length of 40 mm), with the spark gap varying in the range 0.5–2.0 mm (the larger gaps were used to ignite flames at the large Markstein number conditions that were observed for fuel-rich mixtures where ignition energies become quite large). The spark energy was supplied by a high-voltage capacitor discharge circuit having a variable capacitance (100–7000 pF) and voltage (0–10 kV), and a discharge time of roughly 5  $\mu\text{s}$ . Spark energies were adjusted by trial so that they were close to the minimum ignition energy (5–20 mJ, with the larger values used at fuel-rich conditions) in order to minimize effects of initial flame acceleration due to excessive spark energies.

## Instrumentation

The measurements involved observing the flames using shadowgraph motion picture photography. The shadowgraph system was based on a 100 W mercury short arc lamp (ARC, HSA-150 HP), with the light collimated by a pair of f6 parabolic reflectors having focal lengths of 1220 mm. The flame images were recorded using a 16 mm motion picture camera (Hycam, Model K20 S4E) operating at speeds of 5000–6000 pictures per second to yield exposure times as short as 16–20  $\mu\text{s}$ . Kodak Plus X reversal film was used for the photographs. The framing rate of the camera was sensed electronically so that ignition only occurred when the proper framing rate was reached. The framing rate and the ignition

pulse were recorded using a digital oscilloscope (LeCroy 9400A) so that film records could be synchronized.

The film records were measured by projecting them using an Athena Model 224 (MK VIII) projector with an overall magnification of the projected images of 4:1. The flames were nearly spherical (maximum and minimum diameters were within 10% of the mean diameter), but were measured horizontally to avoid the disturbances of the spark electrodes in the vertical direction. The resolution of the flame diameter measurements generally was better than 100  $\mu\text{m}$ .

## Data Reduction

Measurements of laminar burning velocities were limited to flames having diameters less than 60 mm. For such conditions, the volume of burned gas was less than 0.5% of the total chamber volume so that the chamber pressure was constant within 0.7%. Laser velocimeter measurements during earlier work (using a somewhat smaller quasispherical chamber having a 260 mm diameter) indicated that velocities within the unburned gas corresponded to behavior expected for unconfined freely propagating spherical flames [1]. Therefore, it was assumed that effects of motion in the burned gas and flow disturbances due to the presence of the chamber walls were small.

Present measurements were limited to conditions where  $\delta_D/r_f < 2\%$ , which implies negligible curvature and transient effects associated with the thickness of flame, as discussed by Tseng et al. [2]. (Present results formally correspond to use of the hot flame boundary reference frame defined by Clavin [8].) In addition, rates of radiative heat loss were less than 1% of the rate of chemical energy release within the test flames, based on computations assuming adiabatic flame conditions throughout the burned gas region and carried out as discussed by Siegel and Howell [28]. This assessment agrees with an earlier evaluation of radiative effects for hydrogen/air flames at similar conditions due to Dixon-Lewis [29]. Finally, minimum flame radii generally were greater than 5 mm to avoid ignition disturbances and to satisfy the minimum  $\delta_D/r_f$  cri-

terion mentioned earlier. Therefore, effects of energy release due to ignition were small (less than 20 times the energy release due to combustion) for all conditions used to find flame properties. For these conditions, Strehlow and Savage [30] showed that the laminar burning velocity is given by the quasisteady expression

$$S_L = (\rho_b / \rho_u) dr_f / dt, \quad (6)$$

with a corresponding expression for  $K$ ,

$$K = (2/r_f) dr_f / dt. \quad (7)$$

Following past practice [1–3],  $S_L$  was found from Eq. 6 assuming adiabatic combustion at constant pressure with the reactant temperature equal to the initial temperature and with the same fuel-equivalence ratios in the unburned and burned gases. Then, the density ratio needed in Eq. 6 was found by assuming thermodynamic equilibrium in the combustion products for adiabatic, constant pressure and constant fuel-equivalence ratio combustion, using the CEC algorithm of Gordon and McBride [31] and the later STANJAN program of Reynolds [32]—both yielding essentially the same results. It should be noted, however, that this approach represents a *convention* which ignores preferential-diffusion effects that modify the local mixture ratio and thermal energy transport for stretched flames, and thus the local density ratio  $\rho_b / \rho_u$  of the flames. This convention is convenient, however, because a single density ratio is used to relate flame speeds and laminar burning velocities for all levels of flame stretch, which avoids current uncertainties about the effects of stretch on the jump conditions across flames for particular conditions in the unburned gas. Furthermore, the same approach has been adopted during past studies of preferential-diffusion/stretch interactions [1–3, 11–21], which simplifies comparing the various determinations of flame properties. Eventually, a complete description of jump conditions across stretched laminar premixed flames will require information about density ratios as a function of Karlovitz numbers for the reactant mixture conditions of interest. The numerical simulations provide a means of estimating these density ratio variations, but reporting such infor-

mation seems premature at present, pending detailed evaluation of the performance of these simulations over a reasonably broad range of reactant mixture conditions (pressures, compositions, and temperatures). Fortunately, variations of flame properties due to variations of density ratios with stretch do not exceed 11%, based on estimates from the present numerical simulations of the flames, which is comparable to present experimental uncertainties. Finally, it should be noted that the present density ratio convention does not affect the comparison between predicted and measured flame properties, because both are treated in the same way.

Final results were obtained by averaging the measurements of 4–6 tests at each fuel-equivalence ratio considered. Within the range of flame conditions where data were processed, experimental uncertainties (95% confidence) of  $r_f$  were less than 3%, while those of the time and radius differences used to find  $dr_f / dt$  were less than 2 and 5%, respectively. The corresponding uncertainties of  $dr_f / dt$  and  $K$  were less than 9 and 10%, respectively, after allowing for potential effects of unsteadiness, the slight chamber pressure increase due to flame propagation, and radiative heat losses [2, 26]. The present values of  $\rho_u / \rho_b$  and  $D_u$  were assumed to be known so that they do not contribute to uncertainty estimates because they are fixed by *convention* and are tabulated. Then, the previous results imply experimental uncertainties (95% confidence) of  $S_L$  and  $K$  less than 9 and 21%, respectively. The values of  $S_{L\infty}$  and  $Ma$  were found by plotting  $S_L$  as a function of  $Ka$  for each fuel-equivalence ratio, as suggested by Eq. 3. As discussed later, these plots were nearly linear, yielding a constant value of  $Ma$  for  $Ka < Ka_{max}$ , similar to past work [1–3]. This behavior tended to reduce the uncertainties of  $S_{L\infty}$  and  $Ma$  found from least squares fits of these plots, yielding uncertainties (95% confidence) of  $S_{L\infty}$  less than 12% and uncertainties of  $Ma$  less than 25% for  $|Ma| > 1$ , with uncertainties for  $Ma$  increasing inversely proportional to  $|Ma|$  for  $|Ma| < 1$ .

The measurements of Taylor [17] also were reduced using present methods, based on his reported values of flame radius as a function of time. Estimates of experimental uncertainties

were not reported by Taylor [17], but these results appear to be consistent and probably have experimental uncertainties similar to the present investigation.

## Test Conditions

Present test conditions for hydrogen/air flames are summarized in Table 1. The test conditions of Taylor [17] are similar to the present measurements; the original source should be consulted for details.

Table 1 is organized in terms of progressively increasing fuel-equivalence ratios, covering the range 0.30–5.00. It should be noted, however, the first two entries at  $\phi = 0.30$  and 0.45 involve conditions where the limitation  $\delta_D/r_f < 2\%$  was exceeded due to the early appearance of flame wrinkling caused by preferential-diffusion instability, while results at  $\phi = 5.0$  involve conditions where buoyancy affected a portion of the database. Therefore, results at these conditions are provided for informational purposes only. The tabulation

provides, as a function of  $\phi$ , the values of  $\rho_u/\rho_b$  and  $D_u$  used to reduce the data, as well as the resulting values of  $S'_{L\infty}$ ,  $S_{L\infty}$ ,  $\delta_{D\infty}$ ,  $K_{\max}$ ,  $Ka_{\max}$  and  $Ma$ . Values of  $S'_{L\infty}$  were found directly at the largest radius where measurements were made, while values of  $S_{L\infty}$  were found by extrapolating the measurements of  $S_L$  to  $Ka \rightarrow 0$ , similar to past work [1–3], as discussed later. Differences between  $S'_{L\infty}$  and  $S_{L\infty}$  are representative of effects of stretch on the determination of laminar burning velocities that are not corrected for effects of stretch, at least for typical freely (outwardly) propagating spherical laminar premixed flames. These differences tend to be largest near the extremes of the fuel-equivalence ratios, where the absolute values of the Markstein numbers are largest: 20% at  $\phi = 0.30$  and 10% at  $\phi = 5.00$  (both questionable test conditions as noted earlier). Somewhat surprisingly, these differences are comparable or even somewhat smaller than corresponding results for hydrocarbon air flames [2, 3], in spite of the unusually large mass diffusivities of hydrogen which

TABLE I  
Summary of Test Conditions<sup>a</sup>

$\phi$	$\rho_u/\rho_b$	$S'_{L\infty}$ (mm/s)	$S_{L\infty}$ (mm/s)	$\delta_{D\infty}$ ( $\mu\text{m}$ )	$K_{\max}$ ( $\text{s}^{-1}$ )	$Ka_{\max}$	$Ma$
0.30 <sup>b</sup>	3.76	180	150	490	850	0.40	-0.87
0.45 <sup>b</sup>	4.75	470	500	150	4750	0.35	-1.15
0.60	5.56	910	880	80	5560	0.25	-0.80
0.75	6.22	1360	1340	50	2480	0.12	0.25
0.90	6.71	1700	1800	40	3750	0.12	1.09
1.05	6.94	2030	2100	30	5680	0.10	1.72
1.20	6.87	2280	2400	30	5300	0.10	2.80
1.50	6.58	2500	2600	30	5400	0.10	3.35
1.65	6.44	2540	2600	30	5000	0.08	3.50
1.80	6.30	2490	2610	30	4330	0.08	3.72
2.10	6.05	2360	2500	30	4000	0.09	4.26
2.35	5.85	2290	2390	30	4000	0.09	3.46
2.60	5.66	2060	2120	30	3580	0.09	3.90
3.00	5.39	1830	1930	40	2680	0.10	4.27
3.50	5.09	1570	1700	40	1830	0.12	4.79
3.75	4.95	1420	1520	50	1600	0.21	5.00
4.00	4.82	1320	1410	50	1130	0.24	5.51
4.50	4.59	1070	1180	60	780	0.30	5.93
5.00 <sup>c</sup>	4.38	880	980	70	640	0.34	5.99

<sup>a</sup> Hydrogen/air flames at an initial mixture pressure and temperature of 1 atm and  $298 \pm 3 \text{ K}$  ( $D_u = 72.9 \text{ mm}^2/\text{s}$ ).

<sup>b</sup> Provisional results because  $\delta_D/r_f > 2\%$  and  $r_f < 5 \text{ mm}$  for a portion of the data base.

<sup>c</sup> Provisional results because the flame was somewhat distorted by buoyancy for a portion of the data base.

might be expected to cause correspondingly larger preferential-diffusion effects on flame properties. The reasons for this behavior merit additional study.

The characteristic flame thicknesses for unstretched flames listed in Table 1 were found using  $S_{L\infty}$  in Eq. 4, yielding values in the range 30–490  $\mu\text{m}$  (but only 30–80  $\mu\text{m}$  for the range where  $\delta_D/r_f < 2\%$ ). Values based on either the mass diffusivity of oxygen in nitrogen and the thermal diffusivity would be roughly one-third as large. Values of  $\delta_{D\infty}$  based on burned gas conditions would be 3–5 times larger than the values listed in Table 1, yielding characteristic flame thicknesses of 90–400  $\mu\text{m}$  over the present test range (for conditions where  $\delta_D/r_f < 2\%$ ). The relationship between the values of  $\delta_{D\infty}$  summarized in Table 1 and other measures of flame thickness will be considered later when the results of flame structure predictions are discussed. Maximum stretch values were in the range 640–5680  $\text{s}^{-1}$ . However, the corresponding values of the maximum Karlovitz numbers are more meaningful, yielding values in the range 0.08–0.40. These values are relatively small compared to the values on the order of unity that are associated with extinction conditions [10], which is a natural consequence of avoiding large values of  $\delta_D/r_f$  and conditions where effects of the spark disturbances are significant.

A final issue that was considered during the experiments was to assess whether the presence of the minor components of air had a significant influence on the properties of hydrogen/air flames. This question was addressed by carrying out experiments using approximate air (21% oxygen and 79% nitrogen by volume) for comparison with the results for flames using actual air summarized in Table 1. The findings for both hydrogen/air and hydrogen/approximate-air flames are summarized in Table 2 for several fuel-equivalence ratios. The differences between the two sets of results are generally less than 10%, which are comparable to estimated experimental uncertainties. Thus, based on these results, present numerical simulations were simplified to consider only hydrogen/approximate-air flames. An important implication of this finding was that the

**TABLE 2**  
Comparison of Measurements for Hydrogen/Air and Hydrogen/Approximate-Air Flames<sup>a</sup>

Fuel-Equivalence Ratio	2.35	3.75
$S_{L\infty}$ (mm/s)		
Air	2390	1520
Approximate air	2290	1630
Ma		
Air	3.46	5.00
Approximate air	3.92	4.63

<sup>a</sup> Air is normal dry air. Approximate air is 21% O<sub>2</sub> and 79% N<sub>2</sub>, by volume. Tests were carried out at NTP.

complexities of C/H/O chemistry, due to the presence of carbon dioxide in actual air, could be avoided during the present numerical simulations of hydrogen/air flames.

## COMPUTATIONAL METHODS

### Description of Numerical Simulations

The numerical simulations of flames were based on information provided in Refs. 33–38. Simulations of the outwardly propagating spherical flames were carried out using the unsteady, one-dimensional governing equations incorporated in the laminar-flame computer code called RUN-1DL, owing to Rogg [33]. This algorithm allows for mixture-averaged multicomponent diffusion, thermal diffusion, variable thermochemical properties, and variable transport properties. The CHEMKIN package [36] was used as a preprocessor to find the thermochemical and transport properties for RUN-1DL. Except as noted, the transport properties of all species were found following Hirschfelder and Curtiss [39] using the transport property data base of Kee et al. [34], and the thermochemical properties of all species were found from the thermodynamic data base of Kee et al. [35], except for HO<sub>2</sub>, where the recommendations of Kim et al. [5] were used. Prior to computing the results reported here, all transport and thermochemical properties computed in Ref. 36 were checked against original sources. Effects of radiation were small for present test conditions, as noted earlier,

and were ignored. In addition, flame propagation was allowed to proceed sufficiently far during the computations so that effects of the relatively arbitrary initial conditions no longer influenced the predictions—a procedure analogous to the measurements. Finally, other limitations of the analysis of the properties of freely (outwardly) propagating spherical premixed flames apply to the numerical simulations similar to the experiments. Therefore, analysis of the simulated flame properties was limited to  $\delta_D/r_f < 2\%$ , as before.

The numerical algorithm employs self-adaptive gridding to deal with regions where property gradients are large, with the present results based on an Euler extrapolation method; the RUN-1DL manual [33] should be consulted for details. The computational grid in space and time was varied to insure numerical accuracy within 1%, estimated by Richardson extrapolation of  $S_L$ . The numerically simulated results were analyzed similar to the measurements, basing the flame position on the point where the temperature was the average of the hot and cold boundaries. Nevertheless, in view of the relatively stringent flame thickness criterion applied to the computed results, the flames were sufficiently thin in the region of interest so that the results were not very sensitive to the criterion actually used to define the flame position. This routine was used to evaluate the sensitivities of various aspects of the chemical kinetic mechanisms for the Markstein numbers by perturbing reaction rate parameters as discussed later.

A second series of calculations were undertaken for unstretched (plane) flame conditions using PREMIX—the steady, one-dimensional laminar premixed flame code of Kee and co-workers [34–38]. Other properties of these calculations, as well as levels of numerical accuracy, were the same as those using the RUN-1DL algorithm. One difference, however, was that the complete multicomponent diffusion approximation was also considered in this case. In addition, the sensitivities of various aspects of the chemical kinetic mechanisms for the unstretched laminar burning velocities were evaluated using this routine, following Kee and co-workers [37, 38].

### Chemical Reaction Mechanisms

In order to control computer time and costs, only representative recent chemical reaction mechanisms owing to Yetter and co-workers [4, 5] and Wang and Rogg [6] and GRI-Mech 2.1 owing to Frenklach et al. [7] were considered. All these mechanisms are relatively comprehensive and allow for H/O and C/H/O chemistry. Based on the hydrogen/air and hydrogen/approximate-air measurements, however, C/H/O chemistry does not appear to be important for present conditions and was deleted from the mechanisms. In addition, results of Yetter et al. [4] and Kim et al. [5] were essentially the same for present conditions. Therefore, only results for Kim et al. [5] will be considered in the following.

Another concern about the test conditions used for hydrogen/air flames and the chemical reaction mechanisms used to simulate them involved the potential effect of N/O chemistry on the results. This was investigated by carrying out computations both considering and omitting N/O chemistry based on the chemical reaction mechanism of Miller and Bowman [40]. Since C/H/O chemistry was not important for present conditions, however, the prompt NO mechanism was ignored during these considerations. Comparisons between predictions with and without N/O chemistry are summarized in Table 3 for various fuel-equivalence ratios. These results indicate that effects of N/O chemistry are far smaller than experimental uncertainties for the flame prop-

TABLE 3  
Computed Effects of Including N/O Chemistry on Predictions of  $S_L^a$

$\phi$	Ratio <sup>b</sup>
0.5	1.0005
1.0	1.0008
2.0	1.0005
3.0	1.000
4.0	1.000
5.0	1.000

<sup>a</sup> N/O chemistry based on the chemical reaction rate mechanism of Miller and Bowman [40]. Calculations for approximate air at NTP.

<sup>b</sup> Ratio =  $S_{L\infty}(\text{with N/O chemistry})/S_{L\infty}(\text{without N/O chemistry})$ .

erties and conditions of interest during the present investigation. Therefore, N/O chemistry was ignored during subsequent numerical simulations in order to minimize the complexity of the chemical reaction mechanisms.

The final reduced chemical reaction mechanisms (after eliminating C/H/O and N/O chemistry as just discussed) involved 9 species and 19 reversible reactions for the approach of Kim et al. [5], 17 reversible reactions for the approach of Wang and Rogg [6], and 25 reversible reactions for GRI-Mech 2.1 owing to Frenklach et al. [7], not counting the range of third-body collision efficiencies considered in these mechanisms. Finally, the backward rates for all mechanisms were found from chemical equilibrium considerations using the CHEMKIN package [36].

### Transport Models

Naturally, the specifics of any chemical reaction mechanism are influenced by the treatment of transport [40]. Therefore, effects of various transport models were evaluated before undertaking the present numerical simulations of premixed flame properties. The treatment of mass diffusion was of particular interest because using a complete multicomponent diffusion treatment substantially adds to computation times for outwardly propagating spherical flames, compared to use of the mixture-averaged multicomponent diffusion approximation. Thus, these effects were evaluated by computing the variation of unstretched laminar burning velocities with fuel-equivalence ratio using the steady, one-dimensional laminar premixed flame code of Kee and co-workers [34–38] and the chemical reaction mechanism of Kim et al. [5].

The results of the evaluation of the various transport model approximations for present conditions are discussed in the Appendix. The findings agree with the earlier results of Dixon-Lewis et al. [41] and Warnatz [42] for premixed hydrogen/air flames at similar conditions and show that the mixture-averaged multicomponent mass diffusion approximation, including thermal diffusion, was satisfactory for present conditions. Therefore, present cal-

culations were carried out using this approximation in order to control computational costs with little loss of accuracy.

## RESULTS AND DISCUSSION

### Flame Stability and Evolution

Discussion of the results will begin with flame stability characteristics in order to highlight some of the limitations of the present measurements. Three kinds of instabilities were observed during the present experiments: preferential-diffusion instability, hydrodynamic instability, and buoyant instability. Preferential-diffusion instability was of greatest interest because this mechanism involved interactions between effects of preferential diffusion and flame stretch. The relationship between preferential-diffusion/stretch interactions and the stability of thin flames is readily seen from Eqs. 3 and 7. If the Markstein number is negative, the laminar burning velocity increases as the flame stretch (or  $K_a$ ) increases through Eq. 3, then bulges due to disturbances in a nearly smooth flame surface that are concave (convex) toward the combustion products that have positive (negative) flame stretch (or  $K_a$ ), analogous to Eq. 7 for spherical flames, so that the bulges grow and the flame is unstable. Conversely, if the Markstein number is positive, the laminar burning velocity decreases with increasing stretch (or  $K_a$ ), and similar bulges in the flame surface become smaller so that the flame is stable to preferential-diffusion effects. Photographs of outwardly propagating spherical flames for these different preferential-diffusion stability conditions, illustrating this behavior, are reported in Kwon et al. [1].

Two other types of instabilities—hydrodynamic and buoyant instabilities—were observed for stable preferential-diffusion conditions when the flame diameters became large. Hydrodynamic instability involved the appearance of irregular cellular disturbances on the flame surface, similar to those reported by Groff [43]. These disturbances were confined to relatively large flame radii, however, and did not limit present experiments to any extent.

Finally, effects of buoyancy were problematical when the flame radii became large, particularly for slow flames near limits. Nevertheless, these effects were not significant for the present test range due to the imposed flame radius and flame thickness limits of the measurements, except as noted earlier.

Plots of flame radius as a function of time were similar to earlier observations of outwardly propagating spherical flames in this laboratory [1, 2]. Some typical resulting values of  $S_L$  are plotted as a function of  $r_f$  in Fig. 1 for hydrogen/air flames at NTP. Note that some points are included on this plot for illustrative purposes only since they exceed the  $\delta_D/r_f < 2\%$  criterion and were not used to find Markstein numbers and other flame properties. Unstable preferential-diffusion conditions ( $Ma < 0$ ) are denoted by darkened symbols, while stable preferential-diffusion conditions ( $Ma > 0$ ) are denoted by open symbols. All the flames had smooth flame surfaces over the region where measurements are plotted in Fig. 1. Flames at unstable preferential-diffusion conditions, however, developed chaotically irregular surfaces at larger radii; therefore, the plots

are terminated at the last condition where the flame surface was smooth in these cases.

The results illustrated in Fig. 1 show that the effect of flame stretch on laminar burning velocities is substantial, particularly at conditions removed from the neutral-stability condition of  $\phi \approx 0.7$ . For example,  $S_L$  almost doubles for the present range of test conditions as flame radius becomes large at  $\phi = 2.10, 3.50$ , and  $4.00$ . This behavior is not particularly unique to hydrogen/air flames due to the large mass diffusivity of hydrogen. In fact, effects of stretch are similar for hydrocarbon/air flames involving modest variations of mass diffusivities among the reactant species; see Tseng and co-workers [1-3], Taylor and co-workers [16-19], and references cited therein, for examples of these findings. It also is evident that effects of stretch can persist to large flame radii. Due to the small values of  $\delta_D/r_f$  for the present test flames (see Table 1), this behavior is not due to direct effects of flame curvature, i.e., the variation of the cross-sectional area for transport within the thickness of the flame. Instead, it is caused by flame stretch due to the outward motion of a thin curved flame surface, which pushes the unreacted gas ahead of it and strains this gas because the surface area of the flame progressively increases with increasing time.

### Burning Velocity Stretch Interactions

Results for finite flame radii, e.g., Fig. 1, involve finite values of  $K$  so that at the largest  $r_f$  observed,  $S'_{L\infty}$  still differs from the fundamental unstretched laminar burning velocity of a plane flame,  $S_{L\infty}$ . Thus, values of  $S_{L\infty}$  were found through Eq. 3 by plotting  $S'_{L\infty}/S_L$  as a function of  $Ka$  similar to earlier work [1-3]. This yielded a linear plot so that extrapolation to  $Ka = 0$  gave  $S'_{L\infty}/S_{L\infty}$  and thus  $S_{L\infty}$ . This procedure was used to find the values of  $S_{L\infty}$  and the corresponding values of  $\delta_{D\infty}$  summarized in Table 1. Then given  $S_{L\infty}$  plots of  $S_{L\infty}/S_L$  as a function of  $Ka$  can be constructed for various values of  $\phi$  as suggested by Eq. 3. A sample of such results for  $\phi = 0.45, 0.60, 0.75, 1.05, 1.50$ , and  $3.50$  is illustrated in Fig. 2. Results at the other test conditions summarized in Table 1 are similar but have not been

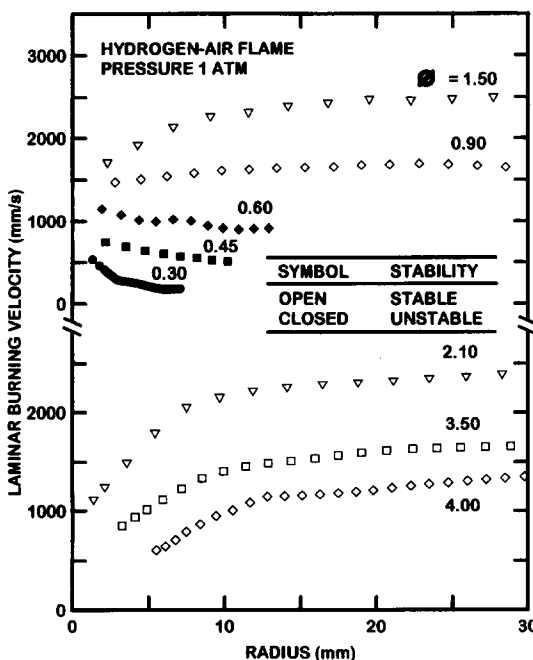


Fig. 1. Measured variation of laminar burning velocities with flame radius for hydrogen/air flames at NTP and various fuel-equivalence ratios.

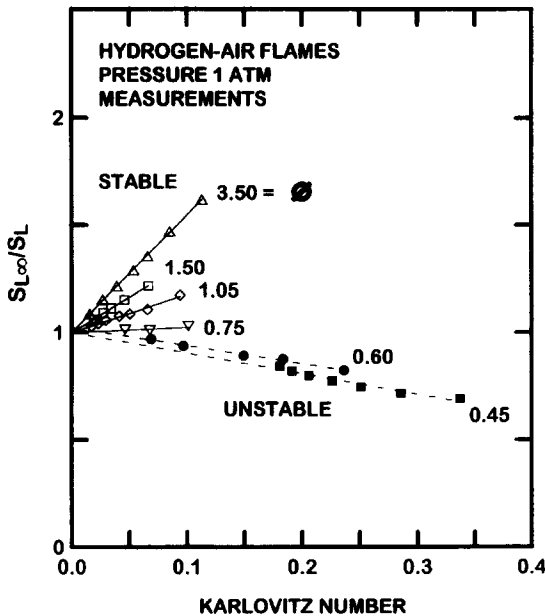


Fig. 2. Measured laminar burning velocities as a function of Karlovitz number and fuel-equivalence ratio for hydrogen-air flames at NTP.

plotted in Fig. 2 in order to avoid overlapping measurements. Similar to Fig. 1, unstable and stable preferential-diffusion conditions are denoted by darkened and open symbols, respectively.

The measurements illustrated in Fig. 2 exhibit the linear relationship between  $S_{L\infty}/S_L$  and  $Ka$  that was exploited to find  $S_{L\infty}$  and has been observed in earlier work by Tseng and co-workers [1–3]. In addition, the slope of these plots, which is equal to the Markstein number from Eq. 3, clearly is independent of  $Ka$  over the range of the measurements (which involves  $Ka < 0.4$ ). It should be recalled, however, that this range of  $Ka$  is not close to extinction conditions (where  $Ka$  would be on the order of unity; see Law [10]) where the response of the flames to stretch is likely to change. Even for this modest range of  $Ka$ , however, the variation of  $S_{L\infty}/S_L$  due to effects of stretch is substantial, e.g.,  $S_{L\infty}/S_L$  is in the range 0.7–1.7. Naturally, larger variations of  $S_{L\infty}/S_L$  are possible given larger ranges of  $Ka$  than those used during the present investigation. As noted earlier, neutral preferential-diffusion conditions are observed for  $\phi \approx 0.7$  with unstable and stable conditions at lower and higher values of

$\phi$ , respectively. Finally, the results of Taylor and co-workers [16, 17] were in reasonably good agreement with the present results when processed using present data reduction methods, including the linearity of the plots of  $S_{L\infty}/S_L$  as a function of  $Ka$  and the response of the flames to stretch seen in Fig. 2. These observations will be quantified later when values of  $Ma$  and  $S_{L\infty}$  are presented.

The same analysis as the measurements was carried out for the numerically simulated freely (outwardly) propagating spherical laminar premixed flames. The predicted variations of  $S_{L\infty}/S_L$  as a function of  $Ka$ , for the same conditions as the measurements illustrated in Fig. 2, are illustrated in Fig. 3. Similar to Figs. 1 and 2, unstable and stable preferential-diffusion conditions are denoted by darkened and open symbols, respectively. As an example, results for the Frenklach et al. [7] chemical reaction mechanism are illustrated in Fig. 3. However, findings using the other chemical reaction mechanisms are qualitatively similar (and will be quantified when measured and predicted  $Ma$  are discussed in the next section). In agreement with the measurements, a linear relationship between  $S_{L\infty}/S_L$  and  $Ka$  is ob-

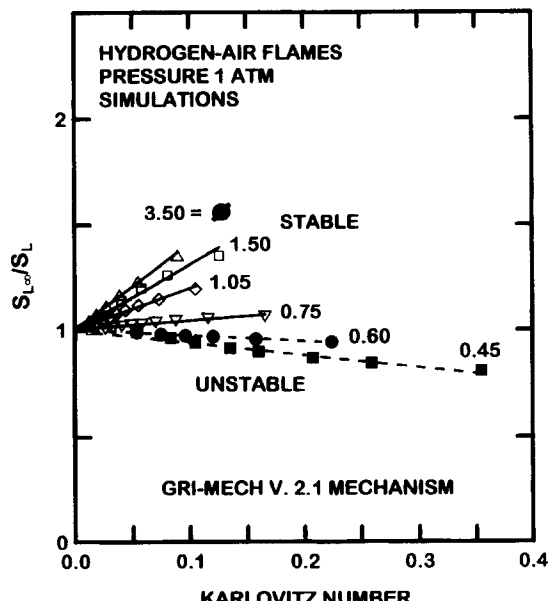


Fig. 3. Predicted laminar burning velocities as a function of Karlovitz number and fuel-equivalence ratio for hydrogen-air flames at NTP. Computations based on the kinetics of Frenklach et al. [7].

tained, implying that Ma is only a function of fuel-equivalence ratio for the present range of conditions. Another point of agreement is that the measured and predicted neutral stability conditions are both at  $\phi \approx 0.7$  with unstable and stable conditions at lower and higher values of  $\phi$ , respectively. Thus, the main difference between measurements and predictions is that the variation of  $S_{L\infty}/S_L$  with Ka is somewhat reduced at small and large values of  $\phi$  for the predictions. This behavior implies somewhat smaller predicted values of Ma (in the absolute sense) than the measurements at these conditions. The evaluation of predicted preferential-diffusion/stretch interactions is seen most concisely from measured and predicted Markstein numbers, however, which are considered next.

### Markstein Numbers

The slopes of the plots of  $S_{L\infty}/S_L$  as a function of Ka yield the Markstein numbers, which are only a function of fuel-equivalence ratio for the present test range. The resulting measured values of Ma are summarized in Table 1 and are plotted as a function of  $\phi$  in Fig. 4. In addition, it should be noted that the present

analysis of the measurements of flame radius data as a function of time owing to Taylor and co-workers [16, 17] yielded essentially the same results as the other measurements, but are not plotted on Fig. 4 to avoid cluttering the figure. Instead, the measurements of Markstein lengths reported by Taylor and co-workers [16, 17] have been converted to Markstein numbers (based on the definition given by Eq. 2) and are illustrated on the plot. These determinations were originally found for the limit of small stretch, but in view of the present findings that Markstein numbers are relatively independent of stretch, the corresponding Markstein numbers should be representative of the range of Karlovitz numbers employed during the present study as well. Finally, the present numerically simulated flames based on the Kim et al. [5], Wang and Rogg [6], and Frenklach et al. [7] chemical reaction mechanisms were analyzed similar to the present measurements and yield Ma predictions that also are shown on the plot.

In view of the importance of hydrogen/air premixed flame properties to developing chemical reaction rate mechanisms needed to complete reliable numerical simulations of flames and the relative novelty of Markstein numbers as a fundamental property of premixed laminar flames, there is an encouraging degree of agreement between the various measured and predicted values of Ma illustrated in Fig. 4. In fact, the measurements agree within experimental uncertainties even though rather different techniques were used to estimate values of Ma for the present study and that of Taylor and co-workers [16, 17]. Due to problems of instability that cause transition to wrinkled flames, the negative Ma region could not be pursued very far. Nevertheless, all the results suggest  $Ma \approx -1$  at the lowest values of  $\phi$  that were considered ( $\phi = 0.30$ ), with neutral conditions ( $Ma = 0$ ) at  $\phi \approx 0.7$ . As  $\phi$  increases beyond the neutral conditions, Ma reaches a plateau value near 5 for a rather broad range of  $\phi$ , e.g.,  $2 \leq \phi \leq 5$ , even though flammability limit conditions were not approached during present tests. The values of  $Ma \approx 5$  at fuel-rich conditions are large and can create problems for measuring the fundamental laminar burning velocities of un-

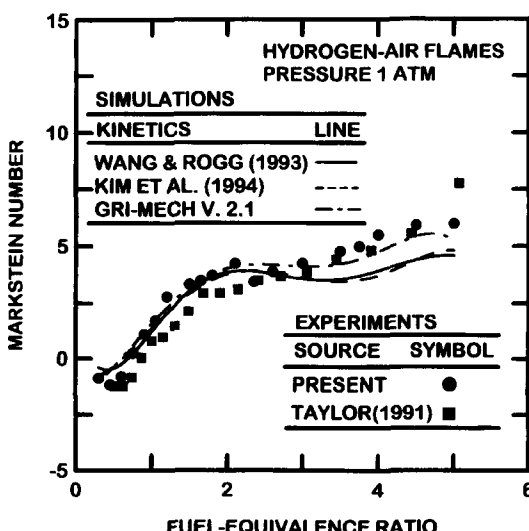


Fig. 4. Measured and predicted Markstein numbers as a function of fuel-equivalence ratio for hydrogen/air flames at NTP. Measurements from Taylor [17] and present study; predictions based on the kinetics of Kim et al. [5], Wang and Rogg [6], and Frenklach et al. [7].

stretched (plane) flames. Nevertheless, even larger values of Ma have been observed for hydrocarbon/air flames, where the reactants have relatively modest mass diffusivity differences [2, 3]. Therefore, large variations of the mass diffusivities among the reactant species are not necessarily a prerequisite for strong preferential-diffusion stretch interactions. The predicted variations of Ma with  $\phi$  in Fig. 4 are similar using all three chemical reaction mechanisms, with the approach of Frenklach et al. [7] yielding somewhat better agreement with measurements than the rest at fuel-rich conditions.

### Unstretched Laminar Burning Velocities

Various reported values of laminar burning velocities of hydrogen/air mixtures at NTP are plotted in Fig. 5. Results that are not corrected for stretch are indicated by open symbols and include the measurements of Andrews and Bradley [44], Bartholome [45], Burwasser and Pease [46], Edmondson and Heap [47], Fine [48], France and Pritchard [49], Fukutani et al. [50], Gibbs and Calcote [51], Gunther and Janisch [52, 53], Heimel [54], Iijima and Takeno [55], Jahn [56], Koroll et al. [57], Liu and MacFarlane [58], Manton and Milliken [59], Payman [60], Scholte and Vaags [61], Senior [62], Smith [63], and Takahashi et al. [64]. These experiments involved a variety of burners, propagating flame test conditions, and methods of data reduction; original sources should be consulted for details. Results that have been corrected for stretch are indicated by darkened symbols and include the measurements of Taylor and co-workers [16, 17], Law and co-workers [11–13] (note that the most recent results of these workers, Ref. 13, have been used at very lean conditions), and the present investigation. As mentioned earlier, the results of Taylor and co-workers [16, 17] were found using freely (outwardly) propagating spherical laminar premixed flames, but with a different extrapolation procedure to estimate results for the plane flame conditions than the present investigation. The measurements of Law and co-workers [11–13] involved a much different extrapolation procedure to estimate the laminar burning velocities of unstretched (plane) flames based on measurements using an opposed-jet configuration.

Although the test configurations and methods of correcting for stretch differ for the results of Taylor and co-workers [16, 17], Law and co-workers [11–13], and the present investigation, the values of  $S_{L\infty}$  from these studies plotted in Fig. 5 agree within experimental uncertainties over the available test range. In addition, present analysis of the measurements of flame radius as a function of time due to Taylor and co-workers [16, 17], yielded results (not shown in Fig. 5) that also agreed with the other stretch-corrected findings within experimental uncertainties. Thus, the stretch-corrected measurements of  $S_{L\infty}$  in Fig. 5 appear to be repeatable. In addition, some of the existing measurements that have not been corrected for stretch, e.g., the results of Fine [48], Jahn [56], Scholte and Vaags [61], and Senior [62], also are in reasonably good agreement with the stretch-corrected measurements. Reasons for this behavior have not been identified at the present time, although the fact that stretch corrections for hydrogen/air flames are modest in comparison to corrections observed for some hydrocarbon/air

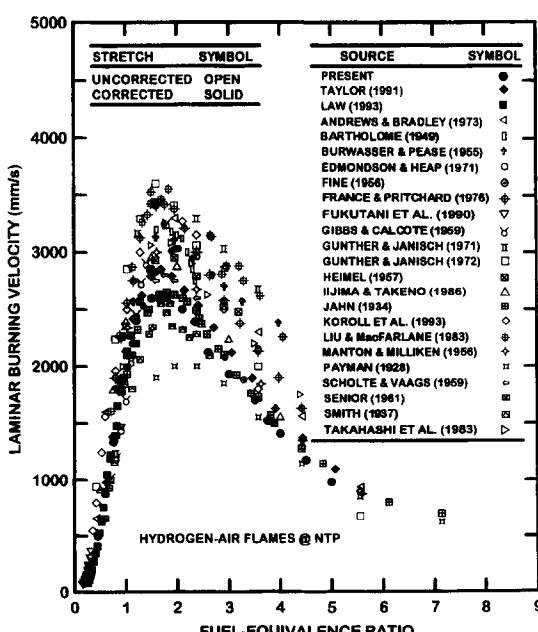


Fig. 5. Corrected and uncorrected measurements of laminar burning velocities as a function of fuel-equivalence ratio for hydrogen/air flames at NTP.

flames (as noted earlier) is undoubtedly a contributing factor.

In spite of the agreement between measurements of unstretched laminar burning velocities of hydrogen/air flames, with and without stretch correction in some instances, most of the measured values of unstretched laminar burning velocities without stretch corrections illustrated in Fig. 5 are significantly larger than the stretch-corrected results. This behavior is particularly evident at fuel-rich conditions, where the uncorrected results can be up to 100% larger than the stretch-corrected results. A possible explanation for the increased differences between uncorrected and stretch-corrected laminar burning velocities at fuel-rich conditions is that these flames are more sensitive to stretch because Markstein numbers are largest in this region (see Fig. 4), although systematic errors for some techniques may also be a factor; see McLean et al. [18] and references cited therein for a discussion of these issues. Nevertheless, more study is needed to determine the reasons for the large variations of the laminar burning velocities of hydrogen/air flames at NTP seen in Fig. 5.

It was felt that the stretch-corrected measurements of  $S_{L\infty}$  for hydrogen/air flames at NTP were the most reliable. Therefore, these results were used to evaluate predictions based

on numerical simulations of flame properties. Similar to the earlier predictions of Ma, the predicted values of  $S_{L\infty}$  were found by treating predictions of flame radius as a function of time in the same manner as the present measurements.

The stretch-corrected measurements and predictions of  $S_{L\infty}$  are illustrated in Fig. 6. The measurements shown here include those of Taylor and co-workers [16, 17], Law and co-workers [11–13], and the present investigation. The predictions are based on the present numerical simulations using the Kim et al. [5], Wang and Rogg [6], and Frenklach et al. [7] chemical reaction mechanisms as before. As noted earlier, the measurements generally agree within experimental uncertainties. Over the fuel-equivalence ratio range of 0.5–1.5, the agreement between all the predictions and the measurements is reasonably good. Furthermore, all the predictions and measurements indicate maximum laminar burning velocities for unstretched hydrogen/air flames at NTP in the range of  $1.5 \leq \phi \leq 2.0$ . On the other hand, discrepancies between the various predictions and measurements are somewhat larger for  $\phi > 1.5$ . These larger discrepancies may be due to greater effects of flame/stretch interactions or larger Markstein numbers in this region as suggested by the results illustrated in

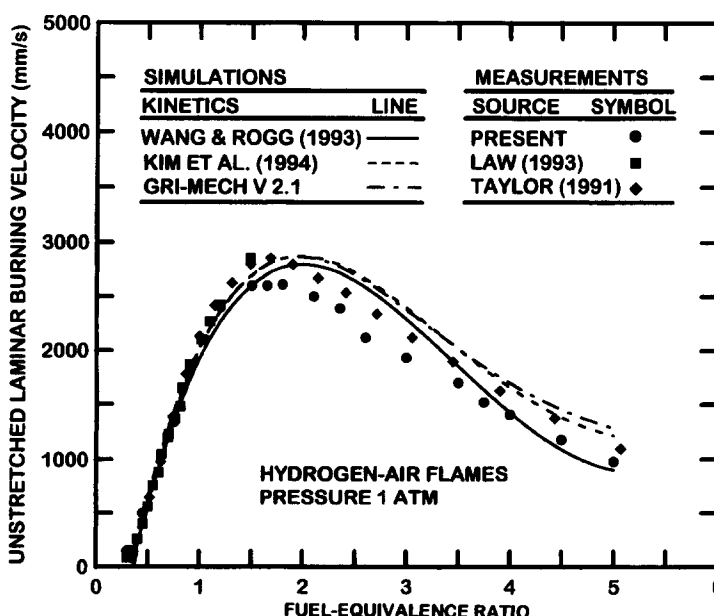


Fig. 6. Measured and predicted unstretched laminar burning velocities as a function of fuel-equivalence ratio for hydrogen/air flames at NTP. Measurements from Taylor [17], Law and co-workers [11–13], and the present study; predictions based on the kinetics of Kim et al. [5], Wang and Rogg [6], and Frenklach et al. [7].

Figs. 4 and 5. It should be noted, however, that the variation of predictions and measurements seen at fuel-rich conditions in Fig. 6 is actually significantly smaller than the variation of the measurements alone at comparable conditions seen in Fig. 5. Thus, the chemical reaction mechanisms of Kim et al. [5], Wang and Rogg [61], and Frenklach et al. [7] may very well be satisfactory for some purposes even though additional study and evaluation of the mechanisms and measurements at fuel-rich conditions would be desirable.

### Sensitivity Analysis

In order to provide some insight about the most important chemical reactions needed to predict interactions between laminar burning velocities and stretch for hydrogen/air flames at NTP, sensitivity calculations were carried out using the methods described by Kee et al. [37] and Grcar et al. [38]. The results for the Frenklach et al. [7] chemical reaction mechanism for  $S_{L\infty}$  are illustrated in Fig. 7; findings using the Kim et al. [5] and Wang and Rogg [6] mechanisms were similar. Findings pictured in Fig. 7 are the normalized sensitivities based on the unstretched mass burning rate at  $\phi = 0.4, 0.7, 1.0, 1.8, 3.0$ , and  $4.0$ , which emphasizes results at fuel-rich conditions where the discrepancies between measurements and predictions are greatest. Results are presented in the

figure for the 11 reactions that exhibit the largest sensitivities.

The reactions exhibiting the greatest sensitivities at fuel-rich conditions ( $\phi = 1.8\text{--}4.0$ ) are  $\text{OH} + \text{H}_2 = \text{H} + \text{H}_2\text{O}$ ,  $\text{H} + \text{HO}_2 = \text{OH} + \text{OH}$ ,  $\text{H} + \text{HO}_2 = \text{H}_2 + \text{O}_2$ ,  $\text{H} + \text{O}_2 = \text{O} + \text{OH}$ , and  $\text{O} + \text{H}_2 = \text{OH} + \text{H}$ . Kim et al. [5] attribute moderate uncertainty factors to all these reactions, in the range 1.5–2.0. Therefore, they merit consideration when seeking an explanation for the discrepancies among the various theories and the measurements at fuel-rich conditions. When the combined effect of the sensitivity of the reaction at fuel-rich conditions and the estimated uncertainty factor of the reaction is considered, then the three-body recombination reactions  $\text{H} + \text{H} + \text{M} = \text{H}_2 + \text{M}$  and  $\text{H} + \text{OH} + \text{M} = \text{H}_2\text{O} + \text{M}$  merit consideration as well. In particular, third-body collision efficiencies in all reactions of this type have not received extensive study and offer a possible avenue to improve the agreement among the various reaction mechanisms.

Sensitivity considerations were extended to effects of reaction rates on Markstein numbers. This could not be done in the elegant manner described by Kee et al. [37] and Grcar et al. [38] that is used for the laminar mass burning rate because Ma is found by fitting estimates of laminar burning velocities at several different stretch rates, as described earlier. Thus, a brute-force technique was used instead, where the effect of a particular reaction on Ma was evaluated by carrying out a complete series of calculations, as described in connection with Figs. 2 and 3, while perturbing the reaction rate in question. These results then were used to compute normalized sensitivity factors for Ma in the usual manner [37, 38].

Evaluation of the sensitivity of Ma to reaction rate constants was carried out for seven reactions exhibiting large combined effects of sensitivity and uncertainty factor for mass burning rates at fuel-rich conditions for the Frenklach et al. [7] mechanism. The resulting normalized sensitivity factors on Ma are illustrated in Fig. 8 for  $\phi = 1.05, 1.8, 3.0$ , and  $4.0$ . Behavior at fuel-rich conditions is most important to improve predictions for this mechanism

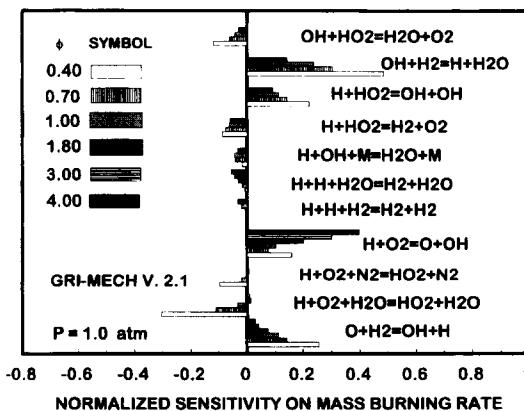


Fig. 7. Normalized sensitivities of kinetic parameters for the unstretched laminar burning velocities of hydrogen/air flames at NTP and various fuel-equivalence ratios. Based on the kinetics of Frenklach et al. [7].

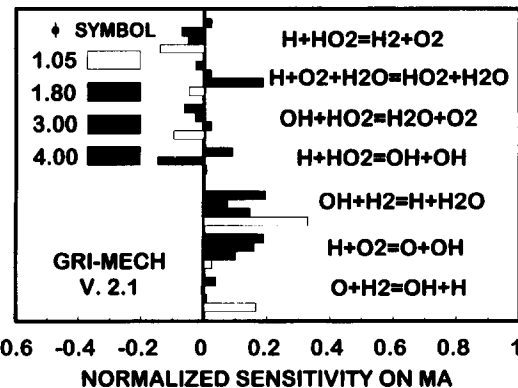


Fig. 8. Normalized sensitivities of kinetic parameters for the Markstein numbers of hydrogen/air flames at NTP and various fuel-equivalence ratios. Based on the kinetics of Frenklach et al. [7].

(see Fig. 4). In this region the  $H + O_2 = O + OH$ ,  $H_2 + OH = H_2O + H$ , and  $H + HO_2 = OH + OH$  reactions exhibit the greatest sensitivities, while  $H + O_2 + H_2O = HO_2 + H_2O$  is important when effects of uncertainty factors are considered as well.

Modifying reaction rate correlations to reduce discrepancies among the various measurements and predictions of both  $S_{L\infty}$  and Ma is a significant task that is beyond the scope of the present investigation. In particular, current discrepancies are not large compared to experimental uncertainties, and consideration of a wide range of experimental conditions, including effects of dilution and pressure, is needed for a definitive exercise along these lines.

### Flame-Structure / Stretch Interactions

As noted earlier, discrepancies between predictions and available measurements of  $S_{L\infty}$  and Ma are comparable to experimental uncertainties. Therefore, use of the predictions to provide information about effects of stretch on flame structure is justified in order to gain a better understanding of laminar-burning-velocity/stretch interactions. Results of this type based on the chemical reaction mechanism of Frenklach et al. [7] are discussed in the following text. Corresponding findings based on the chemical reaction mechanisms of Kim et al. [5] and Wang and Rogg [6] are similar. The ap-

proach involved numerical simulations of outwardly propagating spherical flames for unstable ( $\phi = 0.40$ ), near-neutral ( $\phi = 0.70$ ), and stable ( $\phi = 4.00$ ) preferential-diffusion conditions. The effect of flame-structure/stretch interactions was found by comparing predicted results for a moderate level of stretch ( $Ka \sim 0.1$ ) with corresponding predictions for unstretched (plane) flames.

The predicted structures of stretched and unstretched laminar premixed hydrogen flames at NTP are illustrated in Figs. 9–11 for unstable, near-neutral, and stable preferential-diffusion conditions, respectively. Results illustrated in the figures include distributions of temperature and species mole fractions as a function of distance through the flame. The origins of the length scales for both unstretched and stretched flames in these figures are arbitrary and the latter do not correspond to the center of the outwardly propagating spherical flames.

The first observation of interest with respect to the flame structure predictions of Figs. 9–11 involves the earlier estimates of flame thicknesses summarized in Table 1. These thicknesses are mainly used to estimate unsteady and curvature effects, which are most closely related to density, and thus temperature, variations through the flames. Then defining characteristic flame thicknesses by the total increase and maximum slope of the temperature distribution, the results of Figs. 9–11 yield characteristic flame thicknesses of 300–500  $\mu m$ . Notably, these thicknesses are comparable to estimates based on unburned gas conditions discussed in connection with Table 1.

The way that stretch affects laminar burning velocities is best seen from modifications of radical concentrations in the reaction zone near the hot boundary of the flames. As a first example, consider the near-neutral conditions presented in Fig. 10. In this case, the temperature distributions and maximum temperatures are essentially the same for the stretched and unstretched flames, which results in nearly identical distributions of radicals (compare Fig. 10a and b). As a result, it is not surprising that laminar burning velocities for the two conditions are essentially the same (see Fig. 2) and thus  $Ma \approx 0$ .

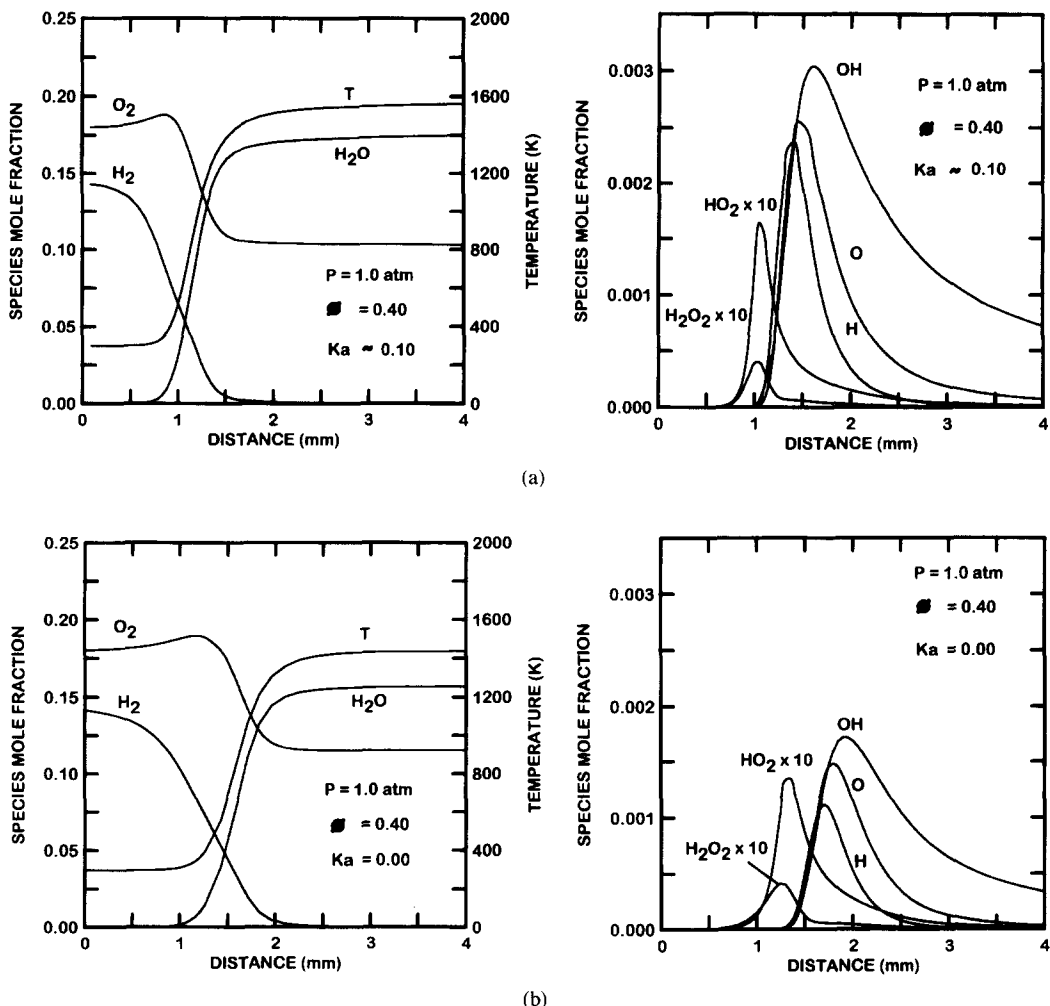


Fig. 9. Predicted structure of (a) a stretched ( $K_a \sim 0.1$ ) and (b) an unstretched ( $K_a = 0$ ) hydrogen/air flame at NTP for unstable preferential-diffusion conditions ( $\phi = 0.40$ ). Based on the kinetics of Frenklach et al. [7].

The response of flame structure to stretch for unstable flames is quite different from near-neutral conditions (compare Figs. 9 and 10). For unstable conditions, finite levels of stretch cause flame temperatures to be higher than for the unstretched flame (roughly 1550 K for the stretched flame in Fig. 9a, compared to roughly 1400 K for the unstretched flame in Fig. 9b). This behavior is caused by effects of preferential diffusion, where the faster diffusion of hydrogen compared to oxygen causes the flame to become more nearly stoichiometric (note the increased concentration of the H<sub>2</sub>O in the combustion products when the flame is stretched); this correspondingly increases the flame temperature when the flame

is stretched. The increased temperature causes radical concentrations in the reaction zone of the stretched flame to increase compared to the unstretched flame (for example, the maximum mole fraction of OH is roughly 0.0032 in the stretched flame (Fig. 9a), but only 0.0018 in the unstretched flame (Fig. 9b)), promoting faster reaction rates and thus higher laminar burning velocities for the stretched flame.

The effect of stretch on flame structure for stable conditions is just opposite to the behavior of unstable flames (compare Figs. 9 and 11). For stable conditions, finite levels of stretch cause flame temperatures to be lower than for the unstretched flame (roughly 1400 K for the stretched flame in Fig. 11a, compared to

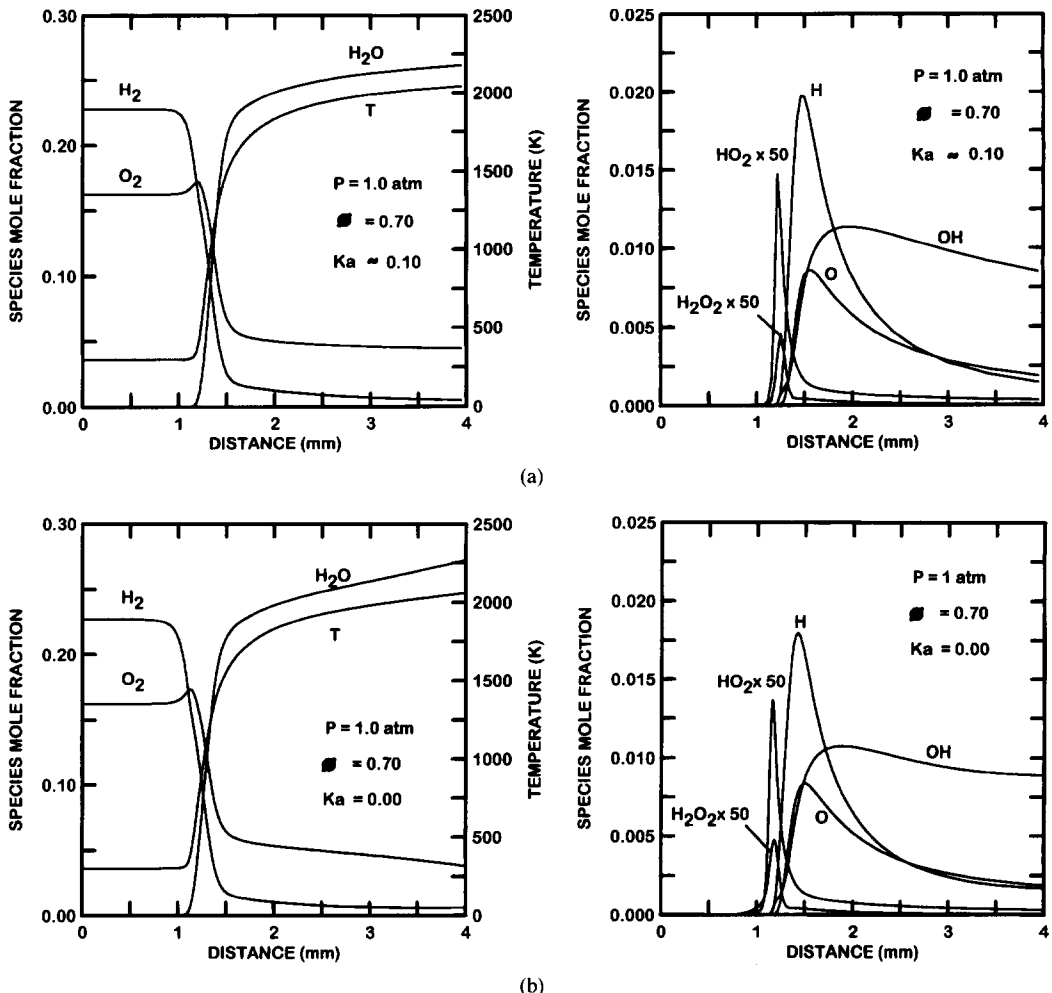


Fig. 10. Predicted structure of (a) a stretched ( $K_a \sim 0.1$ ) and (b) an unstretched ( $K_a = 0$ ) hydrogen/air flame at NTP for near-neutral preferential-diffusion conditions ( $\phi = 0.70$ ). Based on the kinetics of Frenklach et al. [7].

roughly 1500 K for the unstretched flame in Fig. 11b). This also occurs due to effects of preferential diffusion, where the faster diffusion of hydrogen compared to oxygen causes the flame to become richer (note the increased concentration of  $H_2$  and decreased concentration of  $H_2O$  in the combustion products of the stretched flame); this correspondingly decreases the flame temperature when the flame is stretched. The reduced flame temperature causes radical concentrations in the reaction zone of the stretched flame to decrease compared to the unstretched flame (for example, the maximum mole fraction of H is roughly 0.026 in the stretched flame (Fig. 11a), compared to 0.032 in the unstretched flame (Fig. 11b), with similar changes for other radicals),

promoting slower reaction rates and thus smaller laminar burning velocities for the stretched flame.

The effects of stretch on flame structure for hydrogen/air flames at intermediate fuel-equivalence ratios is more complex than the limiting conditions considered in Figs. 9 and 11. In the intermediate regime, effects of preferential diffusion of heat and mass, as well as the propensity for added hydrogen to increase radical concentrations by dissociation to H even though flame temperatures are decreasing, become factors in addition to the effects of preferential diffusion that already have been discussed. Detailed study will be needed to sort out all these effects. Fortunately, the reasonably good performance of the available chemi-

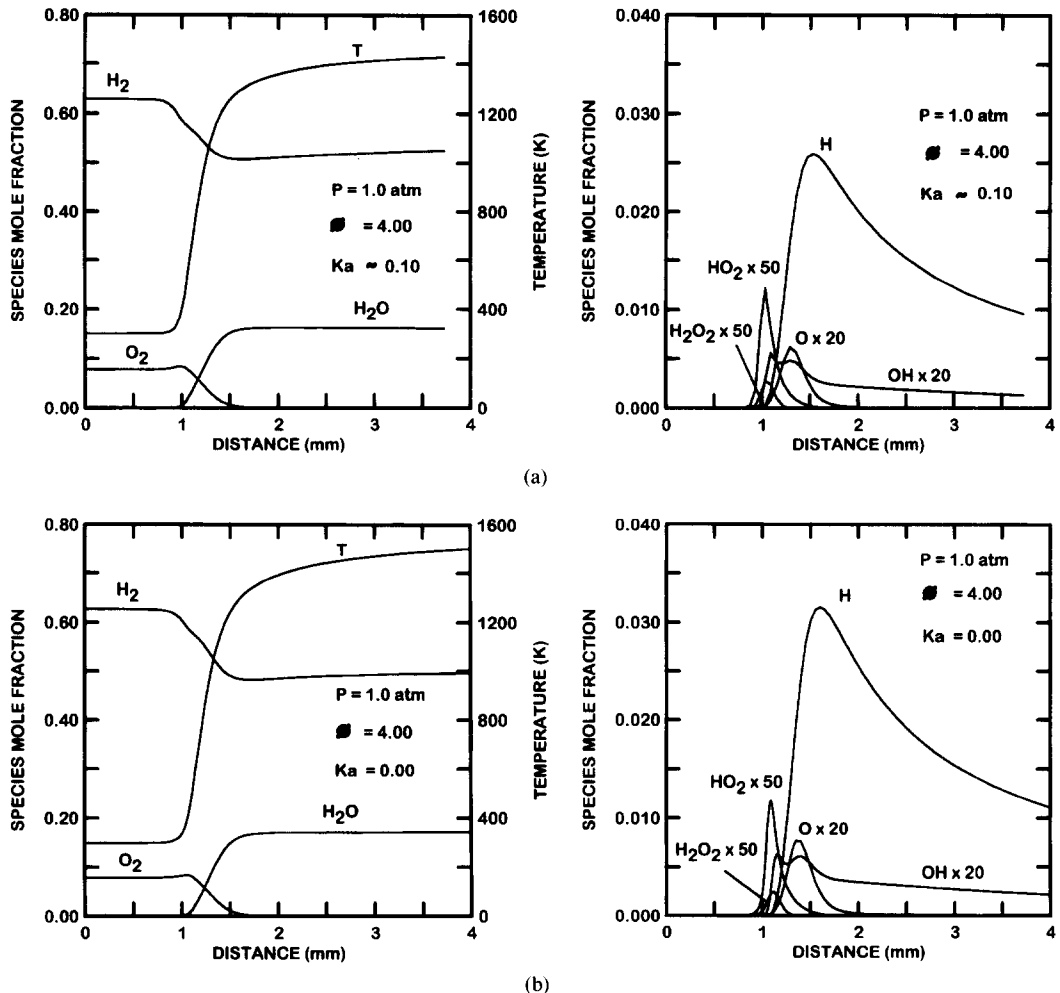


Fig. 11. Predicted structure of (a) a stretched ( $Ka \sim 0.1$ ) and (b) an unstretched ( $Ka = 0$ ) hydrogen/air flame at NTP for stable preferential-diffusion conditions ( $\phi = 4.00$ ). Based on the kinetics of Frenklach et al. [7].

cal reaction mechanisms [5–7] should be helpful for carrying out work along these lines.

## CONCLUSIONS

Effects of positive flame stretch on the laminar burning velocities of hydrogen/air mixtures at NTP were studied both experimentally and computationally. The measurements involved consideration of freely (outwardly) propagating spherical laminar premixed flames based on the methods of Tseng and co-workers [1–3], while the computations involved numerical simulations of the same flame configuration considering the chemical reaction mechanisms of Kim et al. [5], Wang and Rogg [6], and Frenklach et al. [7]. The test conditions in-

cluded fuel-equivalence ratios in the range 0.3–5.0, Karlovitz numbers in the range 0.0–0.4, and laminar burning velocities in the range 100–2700 mm/s. The major conclusions of the study are as follows:

1. Effects of preferential-diffusion/stretch interactions for both the measurements and predictions could be correlated according to  $S_{L\infty}/S_L = 1 + Ma Ka$  to obtain linear correlations between  $S_{L\infty}/S_L$  and  $Ka$ , yielding Markstein numbers that were only functions of fuel-equivalence ratios, similar to past work in this laboratory. However, the applicability of the present approach to general preferential-diffusion/stretch interactions of thin laminar premixed flames is not known and clearly merits additional study.

2. Effects of flame stretch on laminar burning velocities were substantial, yielding Markstein numbers in the range  $-1$  to  $6$  with corresponding variations of  $S_{L\infty}/S_L$  in the range  $0.7$ – $1.7$ . This behavior implies significant effects of flame stretch for typical laboratory measurements of laminar burning velocities as well as for the properties of practical turbulent premixed flames [1].
3. Present measurements of Markstein numbers and fundamental unstretched laminar burning velocities were in good agreement with earlier measurements due to Law and co-workers [11–13] and Taylor and co-workers [16, 17], even though these studies involved different methods of finding parameters associated with preferential-diffusion/stretch interactions. On the other hand, the stretch-corrected values of fundamental unstretched laminar burning velocities generally were smaller than other measurements in the literature, particularly at fuel-rich conditions where Markstein numbers, and thus preferential-diffusion/stretch interactions, are relatively large.
4. Predicted and measured unstretched laminar burning velocities and Markstein numbers exhibited encouraging agreement using the chemical reaction mechanisms of Kim et al. [5], Wang and Rogg [6], and Frenklach et al. [7]. Nevertheless, discrepancies among the various predictions and measurements at fuel-rich conditions merit additional consideration.
5. Predictions of flame-structure/stretch interactions show that unstable ( $\text{Ma} < 0$ ) and stable ( $\text{Ma} > 0$ ) behavior at fuel-lean and fuel-rich conditions, respectively, is explainable by the preferential diffusion of hydrogen compared to oxygen. Behavior at intermediate fuel-equivalence ratios is more complex, however, and involves preferential diffusion of both mass and heat, as well as the effects of the radical-forming propensities of the reactants.
6. Assessment of N/O chemistry based on the numerical simulations and of C/H/O chemistry based on measurements in actual and approximate air suggest that H/O chemistry dominates Markstein numbers and unstretched laminar burning velocities for present test conditions, which simplifies the evaluation of predictions.
7. Preferential-diffusion instabilities caused the appearance and growth of chaotic wrinkled disturbances on the flame surface early in the flame propagation process. The appearance of this type of instability was well correlated by conditions where Markstein numbers were negative. Instabilities still were observed when Markstein numbers were positive; however, they involved irregular cellular-like disturbances that only appeared when flame radii were relatively large, and probably were caused by hydrodynamic instabilities, similar to the earlier observations of Groff [43].
- This research was supported by the National Science Foundation Grant No. CTS-9321959, under the technical management of M. J. Linevsky. Support from the Peace Fellowship Program of Egypt for one of us (M. I. Hassan) also is appreciated. L.-K. Tseng assisted with the initial phases of the research. Useful discussions with B. Rogg also are gratefully acknowledged.*
- ## REFERENCES
1. Kwon, S., Tseng, L.-K., and Faeth, G. M. *Combust. Flame* 90:230 (1992).
  2. Tseng, L.-K., Ismail, M. A., and Faeth, G. M. *Combust. Flame* 95:410 (1993).
  3. Aung, K. T., Tseng, L.-K., Ismail, M. A., and Faeth, G. M. *Combust. Flame* 102:526 (1995).
  4. Yetter, R. A., Dryer, F. L., and Rabitz, H. *Combust. Sci. Tech.* 79:97 (1991).
  5. Kim, T. J., Yetter, R. A., and Dryer, F. L. *Twenty-Fifth Symposium (International) on Combustion*, The Combustion Institute, Pittsburgh, 1994, p. 759.
  6. Wang, W., and Rogg, B. *Combust. Flame* 94:271 (1993).
  7. Frenklach, M., Wang, H., Bowman, C. T., Hanson, R. K., Smith, G. P., Goldin, D. M., Gardiner, W. C., and Lissianski, V., Work in Progress Poster 3–26 at Twenty-Fifth Symposium (International) on Combustion, Irvine, California, 1994; also World Wide Web location <http://www.gri.org/Basic Research/GRI-Mech>, 1995.
  8. Clavin, P. *Prog. Energy Combust. Sci.* 11:1 (1985).
  9. Peters, N. *Twenty-First Symposium (International) on Combustion*, The Combustion Institute, Pittsburgh, 1986, p. 1231.
  10. Law, C. K. *Twenty-Second Symposium (International) on Combustion*, The Combustion Institute, Pittsburgh, 1988, p. 1381.

11. Egolfopoulos, F. N., and Law, C. K. *Twenty-Third Symposium (International) on Combustion*, The Combustion Institute, Pittsburgh, 1990, p. 333.
12. Law, C. K., in *Reduced Kinetic Mechanisms for Applications in Combustion Systems* (N. Peters and B. Rogg, Eds.), Springer-Verlag, Berlin, 1993, p. 15.
13. Vagelopoulos, C. M., Egolfopoulos, F. N., and Law, C. K. *Twenty-Fifth Symposium (International) on Combustion*, The Combustion Institute, Pittsburgh, 1994, p. 1341.
14. Searby, G., and Quinard, J. *Combust. Flame* 82:298 (1990).
15. Deshaies, B., and Cambray, P. *Combust. Flame* 82:361 (1990).
16. Dowdy, D. R., Smith, D. B., Taylor, S. C., and Williams, A. *Twenty-Third Symposium (International) on Combustion*, The Combustion Institute, Pittsburgh, 1990, p. 325.
17. Taylor, S. C., Ph.D. Thesis, University of Leeds, 1991.
18. McLean, I. C., Smith, D. B., and Taylor, S. C. *Twenty-Fifth Symposium (International) on Combustion*, The Combustion Institute, Pittsburgh, 1994, p. 749.
19. Taylor, S. C., and Smith, D. B. *Combust. Flame* 102:523 (1995).
20. Mishra, D. P., Paul, P. J., and Mukunda, H. S. *Combust. Flame* 97:35 (1994).
21. Mishra, D. P., Paul, P. J., and Mukunda, H. S. *Combust. Flame* 99:379 (1994).
22. Markstein, G. H. *Non-Steady Flame Propagation*, Pergamon, New York, 1964, p. 22.
23. Frankel, M. L., and Sivashinsky, G. I. *Combust. Sci. Tech.* 31:131 (1983).
24. Ronney, P. D., and Sivashinsky, G. I. *SIAM J. Appl. Math.* 49:1029 (1989).
25. Matalon, M., and Matkowsky, B. J. *J. Fluid Mech.* 124:239 (1982).
26. Lewis, B., and von Elbe, G. *Combustion, Flames and Explosions of Gases*, 2nd ed. Academic Press, New York, 1961, p. 381.
27. Warnatz, J., in *Combustion Chemistry* (W. C. Gardiner, Jr., Ed.), Springer-Verlag, New York, 1984, p. 197.
28. Siegel, R., and Howell, J. R. *Thermal Radiation Heat Transfer*, 2nd ed., McGraw-Hill, New York, 1981, p. 613.
29. Dixon-Lewis, G. *Combust. Sci. Tech.* 34:1 (1983).
30. Strehlow, R. A., and Savage, L. D. *Combust. Flame* 31:209 (1978).
31. Gordon, S., and McBride, B. J., NASA Report No. SP-273, 1971.
32. Reynolds, W. C. *The Element Potential Method for Chemical Equilibrium Analysis: Implementation in the Interactive Program STANJAN*, Department of Mechanical Engineering, Stanford University, Stanford, CA, 1986.
33. Rogg, B. *RUN-IDL: The Cambridge Universal Laminar Flame Code*, Technical Report CUED/A-THERMO/TR39, Department of Engineering, University of Cambridge, 1991.
34. Kee, R. J., Dixon-Lewis, G., Warnatz, J., Coltrin, M. E., and Miller, J. A. *A FORTRAN Computer Code Package for the Evaluation of Gas-Phase, Multicomponent Transport Properties*, Sandia National Laboratories Report No. SAND86-8246, 1986.
35. Kee, R. J., Rupley, F. M., and Miller, J. A. *The CHEMKIN Thermodynamic Data Base*, Sandia National Laboratories Report No. SAND87-8215B, 1990.
36. Kee, R. J., Rupley, F. M., and Miller, J. A. *CHEMKIN II: A Fortran Chemical Kinetics Package for the Analysis of Gas Phase Chemical Kinetics*, Sandia National Laboratories Report No. SAND89-8009B, 1991.
37. Kee, R. J., Grcar, J. F., Smooke, M. D., and Miller, J. A. *A Fortran Program for Modeling Steady Laminar One-Dimensional Premixed Flames*, Sandia National Laboratories Report No. SAND85-8240, 1993.
38. Grcar, J. F., Kee, R. J., Smooke, M. D., and Miller, J. A. *Twenty-First Symposium (International) on Combustion*, The Combustion Institute, Pittsburgh, 1986, p. 1773.
39. Hirschfelder, J. O., and Curtiss, C. F. *Third Symposium on Combustion and Flame and Explosion Phenomena*, The Combustion Institute, Pittsburgh, 1948, p. 121.
40. Miller, J. A., and Bowman, C. T. *Prog. Energy Combust. Sci.* 15:287 (1989).
41. Dixon-Lewis, G., Isles, G. L., and Walmsley, R. *Proc. Roy. Soc. London Ser. A* 331:571 (1973).
42. Warnatz, J. *Ber. Bunsenges. Phys. Chem.* 82:643 (1978).
43. Groff, E. *Combust. Flame* 48:51 (1982).
44. Andrews, G. E., and Bradley, D. *Combust. Flame* 20:77 (1973).
45. Bartholome, E. *Z. Elektrochem.* 53:191 (1949).
46. Burwasser, H., and Pease, R. N. *J. Am. Chem. Soc.* 77:5806 (1955).
47. Edmondson, H., and Heap, M. P. *Combust. Flame* 16:161 (1971).
48. Fine, B., NACA Report No. TN 3833, 1956.
49. France, D. H., and Pritchard, R. *J. Inst. Fuel* 49:79 (1976).
50. Fukutani, S., Yamamoto, S., and Jinno, H. *Twenty-Third Symposium (International) on Combustion*, The Combustion Institute, Pittsburgh, 1990, p. 405.
51. Gibbs, G. J., and Calcote, H. F. *J. Chem. Eng. Data* 4:226 (1959).
52. Gunther, R., and Janisch, G. *Chemie-Ing.-Tech.* 43:975 (1971).
53. Gunther, R., and Janisch, G. *Combust. Flame* 19:49 (1972).
54. Heimel, S., NACA Report No. TN 4156, 1957.
55. Iijima, T., and Takeno, T. *Combust. Flame* 65:35 (1986).
56. Jahn, G., cited in Lewis, B., and von Elbe, G. *Combustion, Flames and Explosions of Gases*, 2nd ed., Academic Press, New York, 1961, p. 381.
57. Koroll, G. W., Kumar, R. K., and Bowles, E. M. *Combust. Flame* 94:330 (1993).
58. Liu, D. D. S., and MacFarlane, R. *Combust. Flame* 49:59 (1983).
59. Manton, J., and Milliken, B. B. *Proceedings of the Gas Dynamics Symposium on Aerothermochemistry*, Northwestern University, Evanston, 1956, p. 151.

60. Payman, W. *First Symposium on Combustion*, The Combustion Institute, Pittsburgh, 1928, p. 51.
61. Scholte, T. G., and Vaags, P. B. *Combust. Flame* 3:495 (1959).
62. Senior, D. R. *Combust. Flame* 5:7 (1961).
63. Smith, F. A. *Second Symposium on Combustion*, The Combustion Institute, Pittsburgh, 1937, p. 206.
64. Takahashi, F., Mizomoto, M., and Ikai, S., in *Alternative Energy Sources III* (T. N. Veziroglu, Ed.), Hemisphere Publishing Corp., Washington, DC, 1983, p. 447.

Received 15 September 1995; revised 15 June 1996

## APPENDIX

Effects of various transport approximations were evaluated by computing unstretched laminar burning velocities using the steady, one-dimensional laminar premixed flame code of Kee and co-workers [34–37] and the chemical reaction mechanism of Kim et al. [5]. The resulting computed effects of the transport model approximations on the predictions of  $S_{L\infty}$  as a function of  $\phi$  for hydrogen/air flames at NTP are illustrated in Fig. 12. Five sets of calculations are shown, involving progressively more complex treatments of transport, as follows: mixture-averaged multicomponent mass diffusion (MIXA), mixture-averaged multicomponent mass diffusion plus thermal diffusion (MIXA/THDI), complete multicomponent mass diffusion (MULT), complete multicomponent mass diffusion plus thermal diffusion (MULT/THDI), and complete multicomponent mass diffusion plus both thermal diffusion and the Dufour effect (MULT/THDI/DUFO).

The results illustrated in Fig. 12 show that considering the Dufour effect has a negligible influence on predictions of  $S_{L\infty}$ , which is expected because the Dufour effect is higher

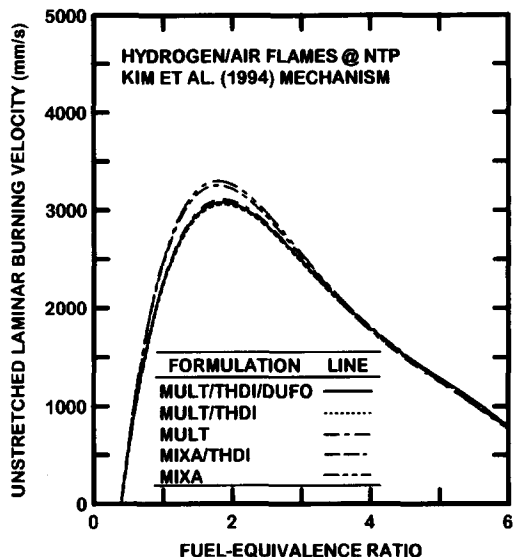


Fig. 12. Effect of transport model approximations on unstretched laminar burning velocity predictions for hydrogen/air flames at NTP. Based on the kinetics of Kim et al. [5].

order than the other transport approximations. Another factor is that mixture-averaged multicomponent mass diffusion and complete multicomponent mass diffusion yield the same results when either including or omitting effects of thermal diffusion. Including effects of thermal diffusion, however, results in a significant reduction of laminar burning velocities near maximum burning velocity conditions ( $1 \leq \phi \leq 3$ ). These observations are in general agreement with the earlier results of Dixon-Lewis et al. [41] and Warnatz [42] for hydrogen/air flames at similar conditions. Based on these findings, computer costs were controlled for computations of these flames with little loss of accuracy by using the mixture-averaged multicomponent mass diffusion approximation while including thermal diffusion.